Available online at www.sciencedirect.com

SciVerse ScienceDirect

Ceramics International 39 (2013) 8219–8226

CERAMICS INTERNATIONAL

www.elsevier.com/locate/ceramint

The effect of bismuth oxide polymorph forms on degradation processes in ZnO varistors

Witold Mielcarek[a,*], Adam Gubański[b], Grzegorz Paściak[a], Krystyna Prociów[a], Joanna Warycha[a], Jerzy M. Wrobel[c]

[a]*Electrotechnical Institute, ul. M. Skłodowskiej-Curie 55/61, 50-369 Wrocław, Poland*
[b]*Wroclaw University of Technology, ul. Wybrzeże Wyspiańskiego 27, 50-370 Wrocław, Poland*
[c]*University of Missouri-KC, 5100 Rockhill Road, Kansas City, MO 64110, USA*

Received 12 February 2013; received in revised form 18 February 2013; accepted 2 April 2013
Available online 9 April 2013

Abstract

The behavior of a ZnO–Bi_2O_3 binary system and ZnO-based varistors under a biasing electric field and temperature was investigated. Both types of samples were exposed to aging with 50 μA DC at 115 °C for 22 h. The degradation effect of DC biasing was manifested by a drop of varistor voltage as well as the presence of peaks in the thermally stimulated discharge current (TSDC) spectra. It was found that the TSDC generation is related to a particular form of the Bi_2O_3 in ceramics. Activation energies of the thermally stimulated responses ranged from 0.01 eV to 0.17 eV. In the high temperature range, the peaks attributable to degradation were found in the TSDC current when the Bi-rich inter-granular phase formed agglomerates and the Bi_2O_3 was in its β- or defective γ- variety. When Bi_2O_3 was in an α-form, well-crystallized γ-form, or an amorphous form, none of the high temperature TSDC maximums were identified. Under a DC bias, the varistor voltage returned to its starting value when the samples were cooled to room temperature. However, passing the current in the opposite direction by reversing the bias from positive to negative exhibited a persistent drop of the varistor voltage.

Keywords: C. Electrical properties; D. ZnO; E. Varistors; Bi_2O_3 polymorphs; Degradation

1. Introduction

Metal oxide varistors are commonly used for the protection of electronic and power devices against voltage surges. Their extensive implementation is a result of their ability to absorb the potentially destructive energy of an incoming transient pulse by changing varistor impedance by many orders of magnitude from a high resistance (about 10^9 Ω) to a highly conductive level, thus reducing the transient voltage to a safe level. Their main drawback of applying is susceptibility to degradation causing an increase in the leakage current at their operating conditions [1] far below the nominal varistor voltage V_n. Since the process is gradual, a failed device is defined by a ± 10% change of the *I–V* characteristics at a 1 mA point [2]. The long-lasting action of an electric field and temperature as well as current surges accelerate degradation of varistors [3–6].

Degradation is strictly connected with fundamental properties of varistor's basic components: ZnO and Bi_2O_3. The non-ohmic behavior of the electric properties of this two component system was discovered by Kossman and Petcsold [7] but it was Matsuoka who enriched it with other metal oxides making it commercially viable [8]. A bismuth film approximately ~5 Å thick is required to create double Schottky potential barriers at the grain boundaries. The height of these barriers is strongly dependent on the excess of oxygen ions at the interface between ZnO grains [9,10]. Therefore the excess of oxygen is essential to the formation of the double Schottky barriers in the varistors, and there is a strong relationship between the drift of oxygen ions and the electrical degradation of the varistors. The diffusion of oxygen ions through the grain boundaries of ZnO contributes to the electrical degradation [10]. Blocking of the drift of oxygen ions by the additive precipitated at the grain boundary can suppress the electrical degradation of varistors [11,12]. In this study we show that the transport of oxide ions through the grain boundaries of ZnO is

*Corresponding author. Tel.: +48 713283061x318; fax: +48 713282551.
E-mail address: mielcar@iel.wroc.pl (W. Mielcarek).

0272-8842/$ - see front matter © 2013 Elsevier Ltd and Techna Group S.r.l. All rights reserved.
http://dx.doi.org/10.1016/j.ceramint.2013.04.006

affected by the crystal structure of Bi_2O_3 particles and related to the ionic conductivity of a particular crystalline phase of the Bi_2O_3 rich intergranular layer.

There are four crystal forms which Bi_2O_3 can take during the varistor sintering. The monoclinic α Bi_2O_3 is stable at room temperature. The metastable tetragonal β and cubic γ forms appear at 650 °C and 635 °C respectively and transform to cubic δ at 730 °C. The δ is stable until oxide fusion at 825 °C when it evaporates as a type of Bi_2O_4 which covers the walls of the furnace [13]. As the furnace is cooling, the α phase reappears at 500 °C [13]. However, all four polymorph forms of Bi_2O_3 have been observed in Bi_2O_3 doped ZnO varistors. The transition of α to γ occurs during the post-processing thermal treatment of varistors [13-16]. The crystal structure of Bi_2O_3 at the grain boundary changes from α to δ due to the addition of Al or Si or by quenching [10]. Both the γ-phase and the α-phase are characterized by low ionic conductivity. In contrast, the δ-phase and the β-phase are good ionic conductors, which intensifies the oxygen migration from the grain boundaries.

The changes in varistor microstructure caused by degradation can be identified by spectroscopic methods of surface analysis. The important finding from X-ray Photoemission Spectroscopy (XPS) studies is that the concentration of oxygen ions adsorbed at the grain boundaries decreases under the force of the electric field [10,17].

The field induced thermally stimulated discharge current (TSDC) method is just a general technique of investigating the electrical properties of high resistivity solids via the study of thermal relaxation effects. This method is used for the study of the charge storage mechanism in dielectric materials. The motion of free carriers is a conduction process which, because of the blocking characteristic of the electrodes, gives rise to the high temperature peak.

The TSDC peak, attributable to the ion migration, disappears from the spectrum after a post-processing thermal treatment of the varistors at 600–750 °C [18,19]. During this treatment, the oxygen high conductive β-Bi_2O_3 transforms into the low conductive γ-Bi_2O_3. As a result the varistor's *I–V* characteristics stabilize at the expense of the varistor non-linearity coefficients [20]. In our previous research [20] on the effect of additional annealing on the crystalline microstructure of ZnO varistors, we concluded that the improvement of the stability of the *I–V* characteristics must result from the low ion (oxygen) conductivity of γ-Bi_2O_3 and the considerably narrower distribution of crystallite sizes after this post-processing annealing. However, we are yet to find the cause of the decrease of the non-linearity coefficients. In the current study, the correlations between Bi_2O_3 polymorph forms and degradation processes in varistors were investigated further.

2. Experimental

2.1. Samples

Three different types of samples were studied in this experiment: ZnBiO, V59 and VBiSnO. The ZnBiO contained the two basic components of a varistor, ZnO and Bi_2O_3. The V59 sample was composed and prepared according to the typical procedures used for fabrication of commercial varistors. In VBiSnO sample the Bi_2O_3 was replaced by $Bi_2Sn_2O_7$. The substitution of $Bi_2Sn_2O_7$ for Bi_2O_3, allowed to reduce the amount of Bi_2O_3 and other metal oxide additives to an absolute minimum which resulted in the development of a varistor microstructure with a nano-wide Bi-rich intergranular layer. The composition of samples is given in Table 1. The samples were prepared using a conventional ceramic technique. The mixtures were ball-milled in deionized water for 18 h. A binder (7% by weight) was added after drying and the mixtures were sifted through a nylon mesh. The powder was palletized into discs 15 mm in diameter and 2 mm thick. The discs were placed in a furnace for sintering. The temperature in the furnace was increased at a rate of 3 °C per minute up to 1250 °C and kept at this temperature for 1 h. Then the samples were cooled in the furnace. In order to get the γ-Bi_2O_3, the varistor sample V59 was annealed at 650 °C and again cooled in the furnace to the room temperature (V59a).

To observe the basic phenomena occurring at the ZnO grain boundaries, the ZnBiO, sample was subjected to heating to 800 °C and subsequently to 884 °C. Prior to heating to 884 °C, the sample was furnace cooled to 740 °C and quenched in an open air.

2.2. Analytical procedures

The microstructure of the samples was examined using scanning electron microscopy (SEM) Jeol JSM-5800 instrument with Energy Dispersive Spectroscopy (EDS) system attached. The crystal phases in the samples were identified with X-ray diffraction (XRD) using DRON-2 powder diffractometer with Fe filtered Co radiation. The XRD patterns were recorded in a scan mode so that $\Delta 2\Theta = 0.05^{\circ}$, and then compared to reference patterns from the Powder Diffraction Files (PDF).

Table 1
Composition of samples.

Denotation of sample	Component [mol%]								
	$BaCO_3$	$Bi_2Sn_2O_7$	Bi_2O_3	Sb_2O_3	Co_2O_3	MnO	Cr_2O_3	NiO	ZnO
ZnBiO	–	–	1.0	–	–	–	–	–	99.0
V59	–	–	1.0	1.0	0.5	0.5	0.4	0.8	95.8
VBiSnO	0.15	0.3	–	0.05	0.5	0.15	–	0.15	98.7

For electrical measurements, gold electrodes were evaporated on the discs' faces. The current–voltage characteristics were taken with an SPEB-1 generator applying a DC current ranging from 10 μA to 5 mA and a pulse current from 5 mA up to 100 A. To study the ageing processes, the samples were subjected to the simultaneous action of electric field and temperature by maintaining 50 μA DC at 115 °C for 22 h and observing the recovery of the varistors voltage during cooling (using METEX 3660 m). The varistors voltage dependence on temperature during cooling from 115 °C to 23 °C were plotted in Arrhenius type graphs. From the slope of the curves, the activation energies of the bulk electron traps were determined. The TSDC measurements were performed in the temperature range from 23 °C to 400 °C. The temperature was increased at a rate of 3 °C/min.

3. Results

3.1. Structural measurements

The ZnO–Bi_2O_3 binary system was examined first. The SEM image of a polished surface of the sintered ZnBiO sample is shown in Fig. 1. The sample was composed of ZnO grains, larger than ten microns, visible in the micrograph as gray areas. The Bi-intergranular phase is also seen in the picture, in the form of white inclusions. The specific composition of this phase, identified by the EDS method, is given in Table 2. As can be seen, in addition to Bi, quite a substantial quantity of Zn, dissolved in Bi_2O_3, was also identified in this phase.

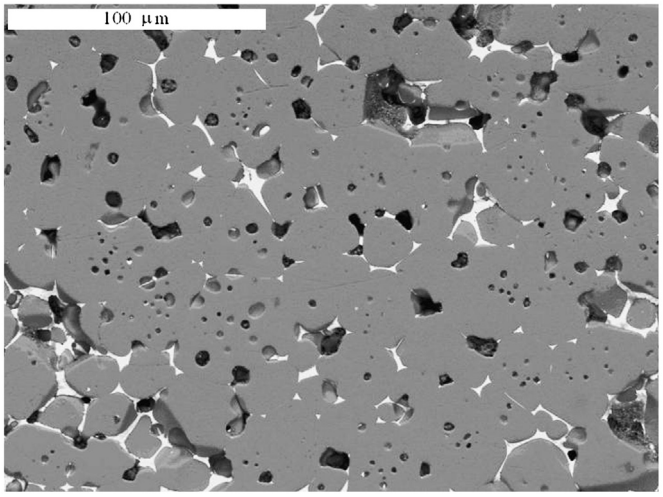

Fig. 1. SEM micrographs of the sintered ZnBiO sample.

Table 2
The chemical composition of the Bi-rich phase of the ZnBiO sample determined by EDS.

Element	Zn	Bi	O
Amount [mol%]	11.54	28.42	60.04

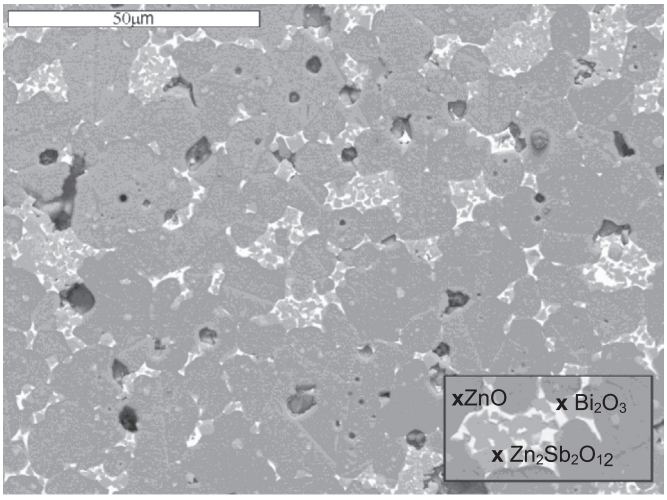

Fig. 2. SEM micrographs of the V59 varistor.

Fig. 2 presents the SEM micrograph of the V59 varistor. The principal constituent of the varistor microstructure, i.e. ZnO grains, are shown as gray spots. The network of white regions around them represents the Bi_2O_3-rich phase. The intergranular Bi_2O_3 phase contains a significant amount of Zn and some amounts of Sb and Cr oxides. The bright gray particles, noticeable in both the Bi_2O_3 phase and ZnO grains, have been identified as a $Zn_7Sb_2O_{12}$ spinel. The majority of metal additives (Bi, Co, Sb, Mn, Ni and Cr) in this varistor appeared to be accumulated in the $Zn_7Sb_2O_{12}$ spinel grains. The chemical composition of the individual phases observed in the V59 varistor's body is presented in Table 3.

The low doped VBiSnO varistor sample exhibits a different type of microstructure. As can be seen in Fig. 3, the SEM image of the thermally etched (at 770 °C for 4 h) sample does not depict intergranular layers or Bi-rich agglomerates. Instead, it shows the intergrain boundaries with pinned point segregates of the intergranular phase.

The few bright clusters, besides Zn and Bi elements, indicate large quantities of Sn and Ba (Table 4). This means that the reaction between them went in the expected direction i. e. the $BaSnO_3$ was synthesized in a reaction of $Bi_2Sn_2O_7$ with $BaCO_3$ liberating the Bi_2O_3 in the effect. The roundness of the segregates is thought to be due to the strong surface tension of the Bi_2O_3 compound.

3.2. Identification of crystal phases

The XRD patterns of the ZnBiO sample are shown in Fig. 4. In the as-sintered sample, the Bi_2O_3 occurred mainly in the α-phase [PDF 27-53]. The post-sintering heating up to 800 °C brought about the crystal γ-phase [PDF 29-235] which remained after returning to room temperature. No significant change in the crystal structure of Bi_2O_3 was observed after reheating to 884 °C and then quenching the sample.

As seen in Fig. 5, in the V59 varistor the β-Bi_2O_3 [PDF 27-50] was identified. After heating at 800 °C, the β-phase recrystallized to γ. The latter phase remained after the sample was

Table 3
Chemical composition of the Bi_2O_3 phase and $Zn_7Sb_2O_{12}$ grains indicated in V59 varistor as determined by EDS.

Investigated phase	Identified elements [mol%]							
	Bi	Sb	Zn	Co	Ni	Cr	Mn	O
Bi_2O_3 (white phase in Fig. 2)	19.2	0.76	13.27	–	–	0.43	–	66.34
$Zn_7Sb_2O_{12}$ (bright gray grains in Fig. 2)	0.16	5.46	18.69	0.58	1.44	1.72	0.70	74.25

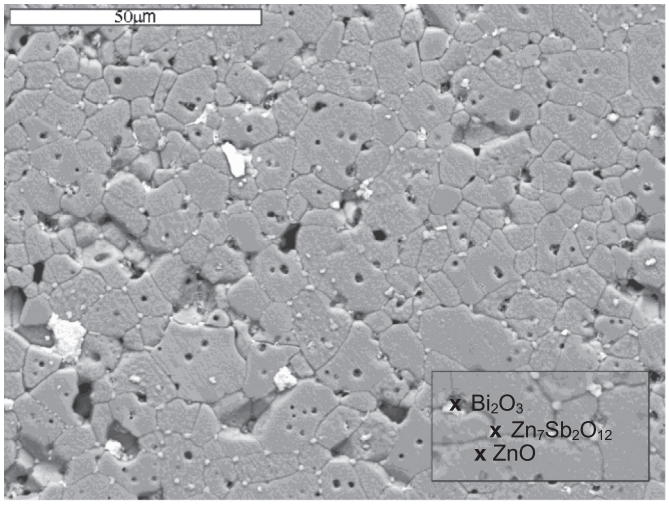

Fig. 3. SEM image of the thermally etched low doped VBiSnO varistor.

Table 4
The chemical composition of the bright phase in the VBiSnO varistor determined by EDS.

Element	O	Zn	Sn	Ba	Bi
Amount [mol%]	48.50	9.19	21.01	19.40	1.90

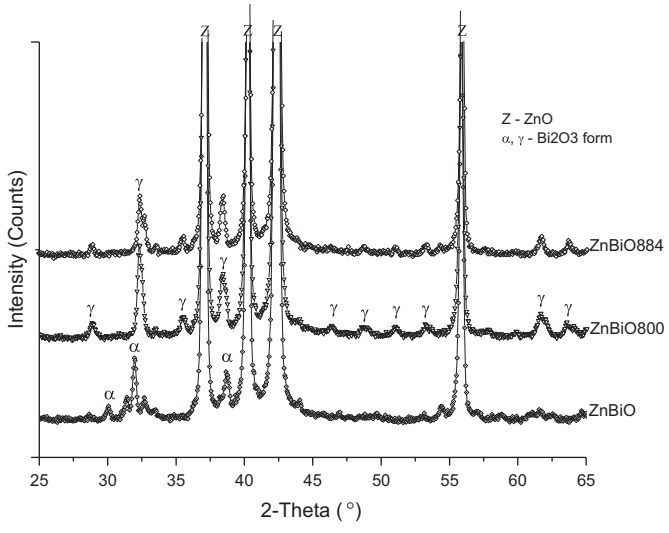

Fig. 4. The XRD patterns of the ZnBiO sample: as-sintered (with α-Bi_2O_3) and after post-sintering heating at 800 °C and 884 °C.

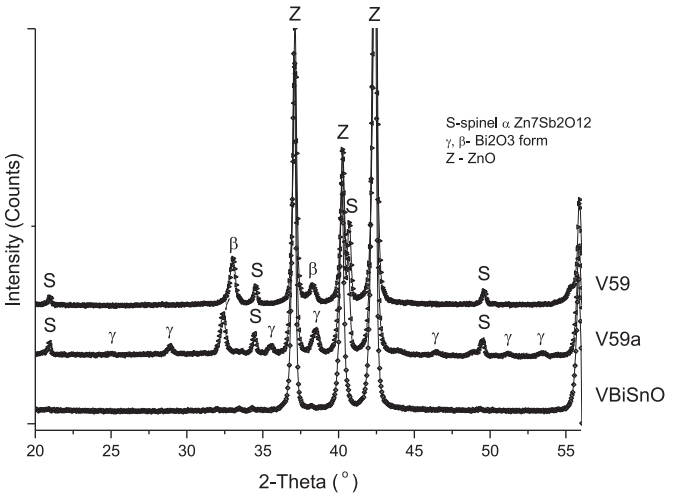

Fig. 5. The XRD patterns of the V59 and VBiSnO varistors.

quenched to room temperature. In the case of the low-doped VSnBiO varistor, none of the Bi_2O_3 crystal phases were identified.

3.3. Electrical measurements

Further investigations concerned the electrical properties of the varistors. As it was mentioned above, the V59 varistor represents a typical ZnO varistor i.e. containing an excess of dopants. Compared to the theoretical estimate, the excess Bi_2O_3 and other dopants in typical varistors is an absolute necessity for developing good varistor properties in the ZnO ceramics. However, it appears that admixturing the ZnO varistors with $Bi_2Sn_2O_7$ instead of Bi_2O_3 enables the possibility of reducing the amount of additives to the theoretical limit. As can be seen in the Fig. 6, adding $Bi_2Sn_2O_7$ has not diminished the varistor property.

The shape of the *I–V* characteristics is typical for varistors. For V59, VBiSnO and ZnBiO varistors, the nominal voltages V_n (at 1 mA) are 194 V, 135 V and 56 V, respectively. Except for the ZnBiO sample, the non-linear exponents were in the range of few tens.

3.4. Varistor reliability

Normally varistors operate at bias voltages below the nominal voltage V_n, and at currents measured in microamperes. The long-term response of a varistor is characterized by a

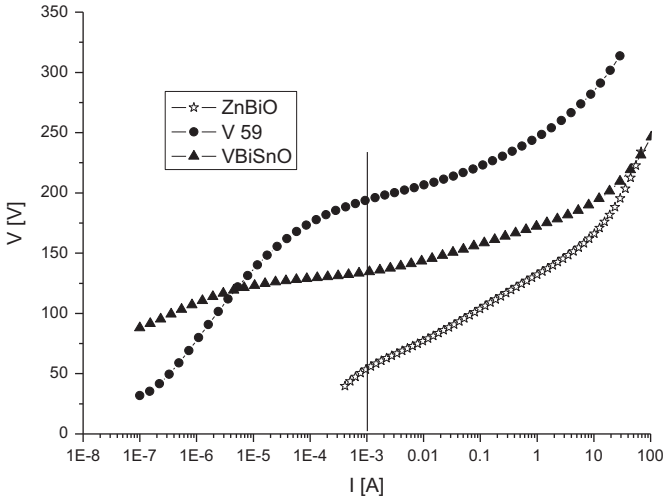

Fig. 6. The *I–V* characteristics of the investigated samples.

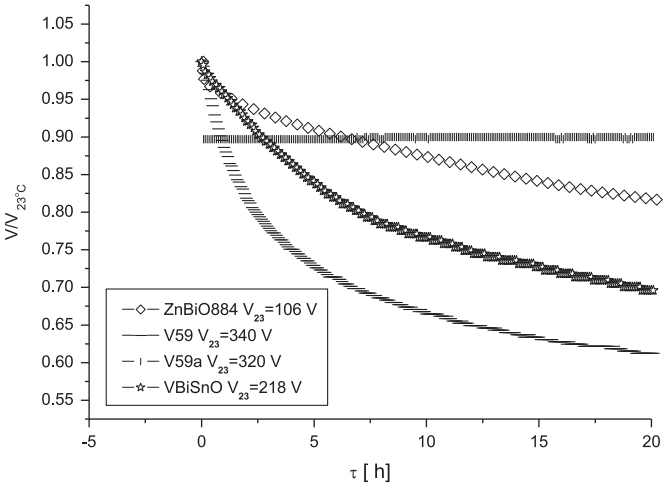

Fig. 7. The relative varistor voltage $V/V_{23\,^{\circ}C}$ as a function of time during ageing with 50 μA dc at 115 °C.

Table 5
Shift in the varistor voltage $V_{50\,\mu A}$ under DC (50 μA) and temperature stressing (115 °C).

Denotation of sample	Bi_2O_3 crystal form in sample	Varistor voltage $V_{50\mu A}$ [V]			
		at 23 °C	at 115 °C 0 h	at 115 °C after 21 h	at 23 °C after ageing under +/−bias
ZnBiO	α	66	58	58	67/62
ZnBiO800	γ	121	98	94	128/93
ZnBiO884	defected γ	106	102	86	102/61
V59	β	340	326	197	334/223
V59a	γ	320	288	287	324/318
VSnBiO	none	218	224	155	220/200

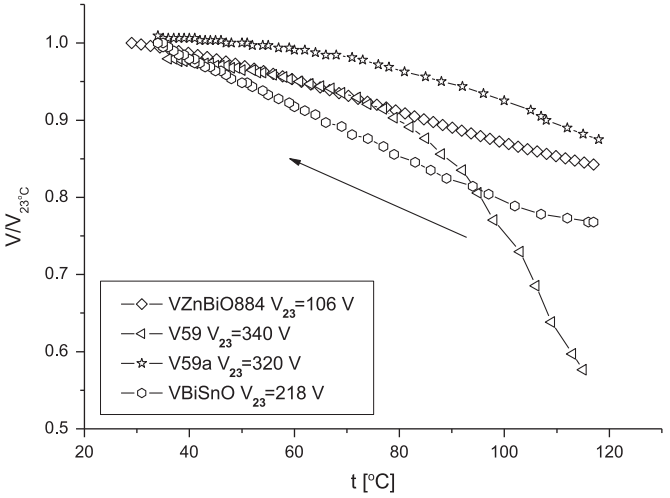

Fig. 8. The relative varistor voltage $V/V_{23\,^{\circ}C}$ as a function of temperature during cooling of degraded samples.

continuous increase in the leakage current. The change in the low voltage leakage current is the most sensitive indicator of varistor degradation as it causes the nominal voltage to fall gradually with time. The definition of failure of a varistor is a drop in the nominal voltage exceeding 10%. Although the varistors are still functioning normally, devices at the lower extreme of the nominal voltage tolerance begin to dissipate more power with the ultimate possibility of a thermal runaway and a varistor failure [6].

As indicated in Table 5, under a combined electro-thermal stress, the varistor voltage ($V_{50\,\mu A}$) across the sample decreases. This drop grows with time. The changes in varistor relative voltage (in relation to the varistors voltage at 23 °C) plotted against time are shown in Fig. 7. The observed degradation process is reversible. After removing the temperature stress, the varistor voltage $V_{50\,\mu A}$ returns to its initial value. However, when the direction of the current is reversed, the varistor voltage shows a persistent drop.

I order to find out if the Bi_2O_3 crystal structure makes any difference in the varistor susceptibility to degradation, the data from Table 5 was also analyzed in reference to the Bi_2O_3 crystal structure. In the ZnBiO sample exhibiting α form of Bi_2O_3, the varistor voltage $V_{50\,\mu A}$ values have not changed significantly during the electro-thermal ageing. The same sample with the Bi_2O_3 phase transformed from α to γ-form, by heating at 800 °C (ZnBiO800), showed a substantial drop in the $V_{50\,\mu A}$ just after being heated to 115 °C (from 121 V at 23 °C to 98 V at 115 °C) and the magnitude of this drop did not change much during further ageing. After removing the temperature stress, whilst retaining the voltage bias, the varistor voltage returned to its initial value. When the direction of the current was reversed, the $V_{50\,\mu A}$ exhibited a persistent drop and the magnitude of this change was substantial. It is worth noting that although no meaningful change in the crystal structure of Bi_2O_3 was observed after the second reheating of the sample to 884 °C (ZnBiO884) and subsequent quenching, the behavior of $V_{50\,\mu A}$ was different and the initial drop of the $V_{50\,\mu A}$ was not sharp but progressed systematically with time. Moreover, as in the previous case, passing the current in the opposite direction by altering the bias terminals from positive to negative showed a large drop of the $V_{50\,\mu A}$.

Both the V59 varistor containing the β-phase of Bi_2O_3 and the low-doped VSnBiO varistor behaved similarly to sample ZnBiO884 during the electro-thermal ageing. However, the persistent drop of the $V_{50\,\mu A}$ in VSnBiO was much smaller and did not exceed 10%. The V59a varistor, obtained by heating the V59 at 800 °C which caused a Bi_2O_3 phase change from β to γ, behaved like the ZnBiO800 during the electro-thermal ageing.

The dynamics of the varistor's recovery during cooling after a thermal stress is shown in Fig. 8. The measurements started at 115 °C and continued down to 23 °C. These measurements also allow calculating the trap energies. Fig. 9 shows a representative Arrhenius plot of the ln(V) against 1/kT generated for the ZnBiO sample heated at 800 °C (ZnBiO800).

In the plot, two straight sections have been distinguished. The high-temperature section ranged from 115 °C to 80 °C, and the low-temperature section ranged from 80 °C to 23 °C. The value of the trap energy can be calculated from the slope of each section. The corresponding trap energies were 0.02 eV and 0.05 eV, respectively Fig. 10.

In a similar way, the trap energies for all the samples were determined and listed in Table 6. Some of these samples exhibited only one trap. The V59 sample, containing the β-Bi_2O_3, showed the highest values of trap energies (0.17 eV). The trap energies of varistor samples with the γ-phase were much lower. Attributing specific trap energy to a particular dopant is not possible because of the complex superposition of the effects originating from different dopants.

As it is generally known [17,18], the degradation effect caused by the field produced by the accumulation of electrons and highly mobile interstitial ions adjacent to grain boundaries, disappears after heat treatment. In this process, the released charge can be measured as the thermally stimulated discharge current. Therefore, the degraded samples were further characterized using the TSDC.

The thermally stimulated release of the built up charge occurred in the ZnBiO884 sample (with the defected γ-phase),

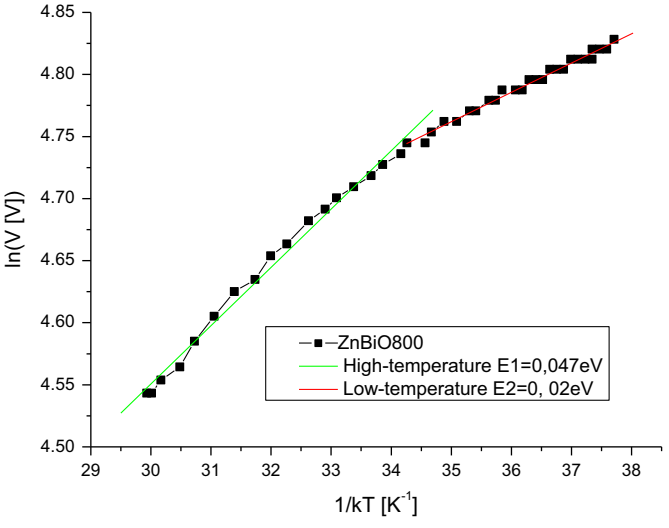

Fig. 9. Determination of the activation energies for sample ZnBiO800 from the Arrhenius plots of the voltage across the varistor during cooling.

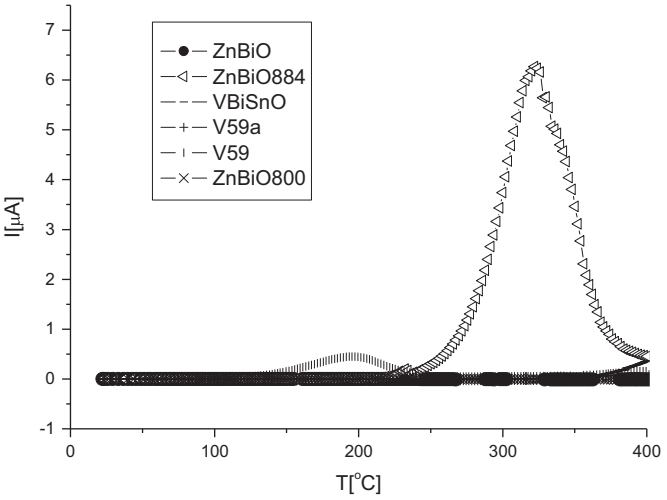

Fig. 10. TSDC spectra of degraded samples.

Table 6
High-temperature ($E1$) and low-temperature ($E2$) trap energy determined from the Arrhenius plots (for forward bias).

Denotation of sample	Bi_2O_3 crystal form in sample	High temperature trap activation energy $E1$ [eV]	Low temperature trap activation energy $E2$ [eV]
ZnBiO	α	–	0.02
ZnBiO800	γ	0.05	0.02
ZnBiO884	defective γ	0.04	0.02
V59	β	0.17	0.01
V59a	γ	0.02	0.005
VSnBiO	none		0.03

Table 7
The parameters of TSDC peaks in degraded ZnBiO884 and V59 samples.

Denotation of sample	Bi_2O_3 form	E [eV]	T_{max} [°C]	I_{max} [μA]
ZnBiO884	γ	1.91	322	6.26
V59	β	0.65	195	0.45

and in the V59 sample (with β-Bi_2O_3). The parameters of the observed TSDC peaks are presented in Table 7. The TSDC spectra of the degraded samples with an α-phase (ZnBiO) and a well-developed γ-phase (ZnBiO800 and V59a), as well as the low doped VSnBiO varistor samples with no Bi_2O_3 crystal phases, did not show any TSDC peaks attributable to the degradation.

These TSDC results support the hypothesis that there is a strong relationship between the drift motion of oxygen ions and the electrical degradation. The degradation process has not been observed when the low-ion conductive crystal phases (α- and γ-Bi_2O_3) segregated to the ZnO grain boundaries and effectively suppressed the diffusion of oxygen ions through the grain boundaries between ZnO grains.

On the other hand, the presence of maxima in the TSDC spectra of the ZnBiO884 sample, with a defected γ-phase, and in the V59 sample, with a β-Bi_2O_3 can be attributed to good

ionic conductivity of these Bi_2O_3 crystal phases. In the case of low doped VBiSnO, the severity of electric and temperature stressing was too low to induce degradation effects detectable with the TSDC method.

4. Summary of results

The dependence of the varistor susceptibility to degradation on Bi_2O_3 polymorph forms was established for three different types of samples. The first was the binary ZnO-Bi_2O_3 system in which non-linear *I–V* properties were discovered by Kossman [7]. The second type of samples, with typical ZnO varistor starting phases described by Matsuoka [8] were composed of ZnO and secondary crystal phases such as β or γ-Bi_2O_3 or $Zn_7Sb_2O_{12}$ spinel. The third consisted of the low doped ZnO varistor with a composition established by the authors. The last samples have not developed any secondary crystal phases during sintering.

The non-ohmic behavior of ZnO varistors is related to the microstructure developed during sintering. The sintering process produces a structure which consists of ZnO grains surrounded by Bi-rich intergranular layers resulting in a network of double Schottky barriers. The *I–V* behavior of varistor is greatly influenced by the barriers. The nature of the barriers is associated with the intergranular layer material doping profile and its thickness. The degradation of the electrical properties of ZnO varistors results from various phenomena occurring at the grain boundaries, such as trap generation or ion migration. These are facilitated by intergranual Bi_2O_3 agglomerates.

The Bi_2O_3 agglomerates emerged in the grain boundary of ZnO–Bi_2O_3 binary system as well as in ZnO doped with Bi_2O_3 and metal oxides which typical for ZnO-based varistors. The useless Bi_2O_3 agglomerates were avoided by admixing ZnO with $Bi_2Sn_2O_7$ instead of Bi_2O_3. This enabled limiting of the amount of dopants to an absolute minimum. Therefore, in the microstructure of the third type, there were no Bi_2O_3 agglomerates.

The degradation phenomena in ZnO varistors result in a continuous increase of the leakage current. The change in the leakage causes the varistor voltage to drop. Cooling the sample to room temperature under a fixed applied current allows the varistor voltage to recover its initial value. The phenomenon of recovery depends on the bias polarization. The varistor voltage recovers only in the case of forward bias. The degradation is related to the low-energy traps ranging from 0.01 eV to 0.17 eV.

The release of charge accumulated in the traps generated by the motion of oxygen ions results in a thermally stimulated discharge current. In varistors with typical composition, as well as in ZnO–Bi_2O_3 binary systems, the TSDC current peaks occur when Bi_2O_3 is in β- or poorly crystallized defected γ-form, both of which are good oxygen conductors. The activation energy of the TSDC peak, observed for samples composed of typical varistor starting phases, was 1.91 eV, and for the ZnO–Bi_2O_3 system, 0.65 eV. Both values correspond to traps associated with the second ionization of oxygen vacancies which are 0.69 eV according to Bueno at al.[9] or 2.0 eV according to Kröger [21]. These support a vacancy mechanism for oxygen diffusion in ZnO, proposed by Sabioni et al. ([22]).

When Bi_2O_3 was in low-conductive forms i.e. in an α well-crystallized γ-form or in an amorphous form, there were no high temperature TSDC peaks. This confirms that varistor susceptibility for degradation strongly depends on the oxygen presence at the interface between ZnO grains, and that the concentration of oxygen is related to the presence of Bi_2O_3 and the particular crystalline form of Bi_2O_3.

Acknowledgments

This work was financially supported by Wroclaw Research Center EIT+ within the project "The Application of Nanotechnology in Advanced Materials" NanoMat (POIG 01.01.02-02-002/08) financed by the European Regional Development Fund (Innovative Operational Programme 1.1.2).

References

[1] K. Sato, Y. Takada, A mechanism of degradation in leakage currents through ZnO varistors, Journal of Applied Physics 53 (12) (1982) 8819–8826.
[2] Transient Voltage Suppression Devices, Harris Cooperation, USA, (1993), p. 3–3.
[3] T.K. Gupta, W.D. Straub, Effect of annealing on the ac leakage components of the ZnO varistor, Journal of Applied Physics 68 (2) (1990) 845–850.
[4] K. Sato, Y. Takada Y, H. Maekawa, M. Ototake, S. Tominaga, Electrical conduction of ZnO varistors under continuous DC stress, Japanese Journal of Applied Physics 19 (5) (1980) 909–917.
[5] S.-N. Bai, T.-Y. Tseng, Degradation phenomena due to impulse-current in zinc oxide varistors, Journal of the American Ceramic Society 78 (10) (1995) 2685–2689.
[6] M.S. Castro, C.M. Aldao, Effects of thermal treatments on the conductance of tin oxide, Ceramics International 22 (1) (1996) 39–43.
[7] M.S. Kosman, E.G. Petcsold, O wozmoznosti izgotowlenija simietriczeskich varistorov iz okisi cinka c primiestju okosi bizmuta Uczonyje zapiski LGPT im, A.I. Gercena 207 (1961) 191–196.
[8] M. Matsuoka, T. Masuyamai, Y. Iida, Non-linear electrical properties of zinc oxide ceramics, Journal of the Japan Society of Applied Physics 39 (1970) 94–101.
[9] P. Bueno, J. Varela, E. Longo, SnO_2, ZnO and related polycrystalline compound semiconductors: an overview and review on the voltage-dependent resistance (non-ohmic) feature, Journal of the European Ceramic Society 28 (2008) 505–529.
[10] F. Stucki, F. Greuter, Key role of oxygen at zinc-oxide varistor grain-boundaries, Applied Physics Letters 57 (5) (1990) 446–448.
[11] M. Takada, H. Yoshino, S.S. Yoshikado, Relationship between grain boundaries and electrical degradation of ZnO varistors, Electrical Engineering in Japan 159 (3) (2007) 105–112.
[12] H. Yoshida, H. Takata, S. Yoshikado, Study on recovery of electrical degradation of ZnO varistors, Key Engineering Materials 350 (2007) 209–212.
[13] E. Dong Kim, M. Yung Hwan, O.H. Chong Hee, Effects of annealing on the grain boundary potential barrier of ZnO varistor, Journal of Materials Science 21 (1986) 3491–3496.
[14] R. Metz, H. Delalu, J. Vignalou, N. Achard, M. Elkhabit, Electrical properties of varistors in relation to their true bismuth composition after sintering, Materials Chemistry and Physics 63 (2) (2000) 157–162.
[15] T. Takemura, M. Kobayashi, Y. Takada, K. Sato, Effects of bismuth sesquioxide on the characteristics of ZnO varistors, Journal of the American Ceramic Society 69 (5) (1986) 430–436.

[16] H. Cerva, W. Russwur, Microstucture and crystal structure of bismuth oxide phases in zinc oxide varistor ceramics, Journal of the American Ceramic Society 71 (7) (1988) 522–530.
[17] M.A. Ramirez, A.Z. Simeos, P.R. Bueno, M.A. Margues, M.O. Orlandi, J.A. Varela, Mechanical properties and dimensional effects of ZnO- and SnO_2-based varistors, Journal of Materials Science 41 (2006) 6221–6227.
[18] M. Nawata, H. Kawamura, M.Ieda, A. Kanematsu, Advances in varistor technology, in: L. Lionel, L.M. Levinson, (Eds.), Proceedings of the 2nd International Varistor Conference, Schenectady N.Y., 1988, Ceramics Transactions. vol. 3, 1989, pp. 186–193.
[19] W. Mielcarek, D. Nowak-Woźny, K. Prociów, A. Gubański, Thermally stimulated currents as measure of degradation of zinc oxide varistors, Radiation Effects and Defects in Solids 157 (2002) 1051–1053.
[20] Y.S. Lee, K.S. Liao, T.Y. Tseng, Microstructure and crystal phases of prazeodymium in zinc oxide ceramics, Journal of the American Ceramic Society 71 (9) (1996) 79–84.
[21] F.A. Kröger S, The Chemistry of Imperfect Crystals, North -Holland Publishing Company, Amsterdam, 1964.
[22] A.C.S. Sabioni, A.M. Daniel, W.B. Ferraz, R.M. Paiz, A.M. Huntz, F. Jomard, Oxygen diffusion in Bi_2O_3-doped ZnO, Materials Research 11 (2) (2008) 221–225.